Appl. Phys. B 69, 71–80 (1999) / Digital Object Identifier (DOI) 10.1007/s003409900063

Applied Physics B
Lasers
and Optics

Thermo-mechanical laser ablation of soft biological tissue: modeling the micro-explosions

B. Majaron[1,*], **P. Plestenjak**[1], **M. Lukač**[1,2]

[1] Jožef Stefan Institute, Jamova 39, SI-1000 Ljubljana, Slovenia
(Fax: +386-61/219-385, +386-61/123-54-00, E-mail: boris.majaron@ijs.si)
[2] Slovenian Development Corporation, Dunajska 160, SI-1000 Ljubljana, Slovenia
(Fax: +386-61/1894-819, E-mail: matjaz.lukac@srd.si)

Received: 9 July 1998/Revised version: 26 February 1999/Published online: 26 May 1999

Abstract. Characteristics of thermo-mechanical laser ablation process are investigated using an original numerical model. In contrast with previous models, it is based on a microscopic physical model of the micro-explosion process, which combines thermodynamic behavior of tissue water with elastic response of the solid tissue components. Diffusion of dissipated heat is treated in one dimension, and the amount of thermal damage is assessed using the Arrhenius model of the protein denaturation kinetics. Influence of the pulse fluence and duration on temperature profile development, ablation threshold, and depth of thermal damage is analyzed for the case of Er:YAG laser irradiation of human skin. Influence of mechanical properties on the ablation threshold of soft tissue is predicted theoretically for the first time. In addition, feasibility of deep tissue coagulation with a repetitively pulsed Er:YAG laser is indicated from the model.

PACS: 81.60.-z; 87.50.Hj; 42.62.Be; 81.40.Gh

The main goal of the presented work is to obtain more realistic predictions of temperature field evolution and the amount of thermal damage in mid-infrared (IR) laser treatment of soft biological tissues, compared to previously presented models. The homogeneous-medium models, for example, which disregard the latent heat of the water-to-vapor phase transition, inevitably predict excessive tissue temperatures above 100 °C. On the other hand, models based on evaporation of tissue water at atmospheric pressure [1–4] are contradicted by experimentally determined values of specific heat of ablation that are lower than the latent heat of evaporation for the corresponding amount of water [5, 6]. Furthermore, ablation temperatures above 100 °C [7–9], dependence of ablation efficiency on tissue tensile strength [5], and histological evidence of tissue tear [8] all indicate that ablation of tissue with free-generating mid-IR lasers is not a purely evaporative process. Supported also by observations from high-speed photography [10] and time-resolved thermometry [9], a concept of micro-explosions is now generally accepted [1, 11]. Such thermo-mechanical ablation mechanism has to be distinguished from mechanisms involving strong acoustic transients, plasma formation, or transient bubble formation, which can be encountered at higher laser intensities.

We introduce a microscopic physical model of the micro-explosion. Thermodynamic behavior of tissue water, which acts as a chromophore for the mid-infrared laser radiation, is combined with elastic response of the surrounding solid medium. This is complemented by one-dimensional treatment of heat diffusion using a finite-difference scheme, and modeling of the protein denaturation kinetics with the Arrhenius integral. The main ideas behind this model and some results have been revealed before in two conference contributions [12, 13]. Here, we explore in more detail physical aspects of the microscopic model of micro-explosions and its implementation. In the discussion of results, we focus on relations between the structure of the model and predicted characteristics of the thermo-mechanical ablation process.

Using the optical, thermal, and mechanical properties of human skin from literature, the model predicts realistic values of ablation temperature, ablation threshold fluence, and coagulation depth for the case of single-pulse irradiation with a free-generating Er:YAG laser. We therefore use the model also to examine the influence of pulse fluence and duration on temperature profile, ablation threshold, and depth of thermal damage. Furthermore, the influence of tissue mechanical properties on mid-IR laser ablation threshold is predicted theoretically for the first time, in good agreement with experimental observations [5].

Some results are presented also for repetitively pulsed irradiation, where the ablation threshold and coagulation depth are calculated for varying numbers of pulses and repetition rate. This is of interest especially for the laser skin resurfacing, where a controlled amount of collagen denaturation (100–200 μm) is recently believed to be beneficial. Currently, the Er:YAG laser is recognized as a premier tool for superficial ablation of cutaneous lesions [14–16], due to extremely strong absorption of its mid-IR ($\lambda = 2.94\,\mu$m) radiation in water. This results in a minimal amount of thermal dam-

* Corresponding author

age to underlying tissue, and faster healing compared to CO_2 lasers [15, 17]. Our results indicate, however, that deep coagulation of cutaneous tissue can be achieved with Er:YAG laser by choosing an appropriate application modality, in agreement with preliminary experimental results [17–19].

1 The model

1.1 Microscopic equation of state

In our model of interaction between mid-IR laser radiation and soft biological tissue, we treat the latter as a two-component medium. As a simplest possible starting point, we postulate that tissue water is trapped in microscopic spherical cavities in a non-absorbing elastic medium. All cavities are initially filled with water at 36 °C and normal atmospheric pressure ($p_0 = 1$ bar). As the water absorbs the laser radiation, its temperature increases linearly until the boiling point ($T_0 = 100$ °C) is reached. Further heating converts one part (x) of the water mass into vapor. As the vapor can not expand freely, pressure in the cavity rises and exerts force on the cavity wall (Fig. 1). The new cavity volume thus depends on both thermodynamics of the water/vapor mixture in the cavity, and elastomechanics of the surrounding medium.

The volume of the cavity V is on one hand thus calculated by adding the vapor and water volume (V_v, V_w). In doing so, density of vapor is estimated using the ideal-gas equation, which is less than 3% off the data in steam tables at 100 °C (and less than 10% off at 200 °C):

$$V = V_\mathrm{v} + V_\mathrm{w} = V_0 \left[\left(\frac{rT\rho_\mathrm{w}}{p} - 1 \right) x + 1 \right] . \tag{1}$$

Here, V_0 marks the initial cavity volume, r is the specific gas constant for water vapor (462 J/kgK), and ρ_w denotes the density of liquid water.

On the other hand, the new cavity volume is related to pressure inside it by the stress–strain relations of the surrounding tissue. For a single spherical cavity in an infinite elastic medium, this relation is derived from the condition of mechanical equilibrium [20] as (see the Appendix):

$$V = V_0 \left[1 + \frac{1+\nu}{2E} (p - p_0) \right]^3 , \tag{2}$$

where E is the Young's modulus of the tissue, and ν marks its Poisson's ratio. After equating the volumes (1) and (2), the unknown initial volume of the hypothetical cavity V_0 cancels out:

$$\left(\frac{rT\rho_\mathrm{w}}{p} - 1 \right) x + 1 = \left[1 + \frac{1+\nu}{2E} (p - p_0) \right]^3 . \tag{3}$$

Assuming that the two phases are in thermodynamic equilibrium at all times, temperature T equals the boiling temperature of water at pressure p. An analytical relation can be derived from the Clausius–Clapeyron equation, in which the vapor density is again expressed from the ideal-gas equation [21]:

$$\frac{\mathrm{d}p}{\mathrm{d}T} = \frac{p\, q(T)}{rT^2} . \tag{4}$$

This can be integrated after replacing the temperature-dependent latent heat of evaporation $q(T)$ with its average value on the interval (T_0, T), resulting in a compact formula

$$\frac{1}{T} = \frac{1}{T_0} - \frac{r}{\bar{q}} \ln \left(\frac{p}{p_0} \right) , \tag{5}$$

which matches well the data in steam tables. The temperature dependence of the latent heat itself is approximated by the linear approximation:

$$q(T) = q(T_0) - (c_\mathrm{w} - c_\mathrm{v})(T - T_0) , \tag{6}$$

where c_w and c_v are (isochoric) specific heat capacities of liquid water and vapor, respectively. By inserting $T(p)$ from (5) into (3), an equation of state (EOS) for our cavity is obtained, which relates cavity pressure p with the relative vapor content x.

1.2 Macroscopic effects, parameters, and implementation

Evolution of temperature field in a laser-irradiated tissue is modeled using the finite-difference method. To that end, the local EOS (3) must be complemented by a relation between the heat ΔQ, delivered to a given computational cell of cross section S and depth Δz in a time step Δt, and the resulting change in the values of local thermodynamic variables:

$$\begin{aligned} \Delta Q = S\Delta z\rho \,[& wq(T)\Delta x + wx(c_\mathrm{v} + r)\Delta T + w(1-x)c_\mathrm{w}\Delta T \\ & - w\Delta p/\rho_\mathrm{w} + (1-w)c_\mathrm{s}\Delta T] . \end{aligned} \tag{7}$$

Here, the first three terms describe the enthalpy changes in additional evaporation, heating of vapor, and heating of water to the new equilibrium temperature. The fourth term is related to work performed on the surrounding tissue (note that for a single cavity, deposited heat and resulting enthalpy change are related as $\Delta Q = \Delta H - V\Delta p$). The last term accounts for eventual conductive thermalization of the solid tissue components within the computational cell.

Diffusion of heat on a macroscopic level is introduced into the model by composing the heat-source term ΔQ from the absorbed laser radiation (according to Beer's law), and conductive heat flow between the surrounding cells in one dimension (z). Solving of the heat-diffusion problem using the finite-difference method is thus interleaved with solving of

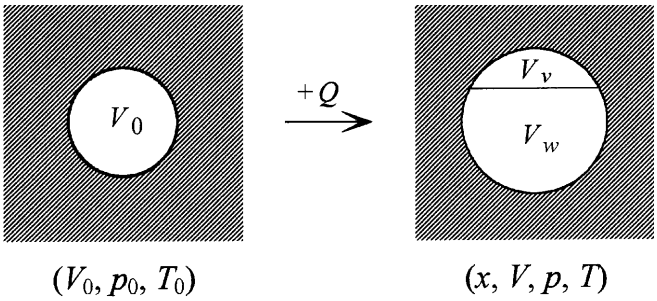

Fig. 1. Illustration of the model. Heat delivered to a water-filled spherical cavity inside an infinite elastic medium converts one part of the water (x) into vapor, resulting in increase of cavity volume, pressure, and temperature

a highly nonlinear set of equations (3), (5), (7), which describe the evolution of local thermodynamic variables, at each spatial position.

We deal with this nonlinearity by replacing Δx and Δp in (7) with $(\mathrm{d}x/\mathrm{d}T)\Delta T$, and $(\mathrm{d}p/\mathrm{d}T)\Delta T$, respectively. Equation (7) thus becomes linear in temperature rise ΔT, and can be reversed:

$$\Delta T = \frac{\Delta Q}{S\Delta z\rho w\left[q(T)\frac{\mathrm{d}x}{\mathrm{d}T} - (c_\mathrm{w}-c_\mathrm{v}-r)x + c_\mathrm{w} + \frac{(1-w)}{w}c_\mathrm{s} - \frac{1}{\rho_\mathrm{w}}\frac{\mathrm{d}p}{\mathrm{d}T}\right]}. \tag{8}$$

The derivative $\frac{\mathrm{d}x}{\mathrm{d}T}$ can namely be expressed analytically from (3):

$$\frac{\mathrm{d}x}{\mathrm{d}T} = \frac{\frac{3(1+\nu)}{2E}\left[1+\frac{(1+\nu)(p-p_0)}{2E}\right]^2\frac{\mathrm{d}p}{\mathrm{d}T}}{\left(\frac{rT\rho_\mathrm{v}}{p}-1\right)} - \frac{\left[\left[1+\frac{(1+\nu)(p-p_0)}{2E}\right]^3-1\right]\frac{r\rho_\mathrm{v}}{p}\left(1-\frac{T}{p}\frac{\mathrm{d}p}{\mathrm{d}T}\right)}{\left(\frac{rT\rho_\mathrm{v}}{p}-1\right)^2}, \tag{9}$$

and $\frac{\mathrm{d}p}{\mathrm{d}T}$ from (4). After the temperature increase ΔT is thus established, new values of p, V, and x are calculated from (5), (2), and (3), respectively.

In addition to the above, the protein denaturation process is modeled at each point in space and time by calculating the damage parameter Ω according to the Arrhenius equation of protein denaturation kinetics:

$$\Omega(z,t) = A\int_0^t \mathrm{e}^{-\frac{E}{RT(z,t')}}\,\mathrm{d}t', \tag{10}$$

with parameter values $A = 3.1\times10^{98}\,\mathrm{s}^{-1}$ and $E = 6.28\times10^8\,\mathrm{J/kmol}$ [22]. As customary, tissue is assumed to be irreversibly modified when Ω exceeds 0.5.

Physical properties of skin used in our numerical model are shown in Table 1. Note especially the two values of the Young's modulus. The strongly nonlinear stress–strain relation of skin is approximated by a low-elastic-modulus region at small deformations, and another linear region with a higher elastic modulus value, encountered when linear extension exceeds 100% [23]. Accordingly, (2) is used with the lower Young's modulus value E_1 until the cavity volume is increased by a factor of 4, when a linear extension of 100% is reached at the cavity wall. At larger cavity volumes, (2) is thus replaced by

$$\frac{V}{V_0} = 3 + \left(1+\frac{1+\nu}{2E_2}(p-p')\right)^3, \tag{11}$$

where p' represents the cavity pressure at the cross-over volume ($4V_0$). Its value is obtained from (2) and inserted into (11), yielding the right-hand-side of EOS (3) appropriate for the higher cavity volumes:

$$\frac{V}{V_0} = 3 + \left[1+\frac{1+\nu}{2E_2}(p-p_0) - \frac{E_1}{E_2}\left(\sqrt[3]{4}-1\right)\right]. \tag{12}$$

The thus obtained p–V relation for the model cavity is illustrated in Fig. 2. The enlarged view of the low-pressure range in the inset shows functions (2) and (12), as well as (p, V) pairs from a specific run of the numerical model using a constant laser intensity and no heat diffusion. The time evolution of cavity state in the same case is presented in Fig. 3, where cavity volume (relative to initial volume V_0), pressure, temperature, and vapor content are plotted as a function of deposited energy density.

The model is solved by a dedicated finite-difference code in Turbo Pascal, run on a personal computer (Pentium 166 or 200). For the single-pulse cases we use a spatial resolution of $\Delta z = 0.5\,\mu\mathrm{m}$ over a depth interval of $50\,\mu\mathrm{m}$. The time step Δt is set to $1\,\mu\mathrm{s}$, in accordance with stability condition of the chosen numerical procedure for solving the heat diffusion equation [24]:

$$\Delta t \le \frac{(\Delta z)^2}{2D}, \tag{13}$$

where D represents the thermal diffusivity of tissue as a whole ($1.1\times10^{-7}\,\mathrm{m^2/s}$). A physical interpretation of this requirement would be that the time step Δt must be short enough to prevent substantial diffusion of heat further than

Table 1. Optical, thermal, and mechanical properties of human skin, used in the numerical calculations

Property	Value
Water content (weight perc.) [23]	$w = 70\%$
Absorption coefficient [25]	$\mu = 300\,\mathrm{mm^{-1}}$
Average density	$\rho = 1100\,\mathrm{kg/m^3}$
Thermal conductivity	$\lambda = 0.42\,\mathrm{W/mK}$
Specific heat capacity of the solid component [23]	$c_s = 1700\,\mathrm{J/kg\,K}$
Young's modulus of elasticity [23]	$E_1 = 0.5\,\mathrm{MPa},\ (\Delta l/l < 1)$ $E_2 = 48\,\mathrm{MPa},\ (\Delta l/l > 1)$
Poisson's ratio	$\nu = 0.5$
Ultimate tensile strength (face) [23]	$\sigma_\mathrm{c} = 3.7\,\mathrm{MPa}$

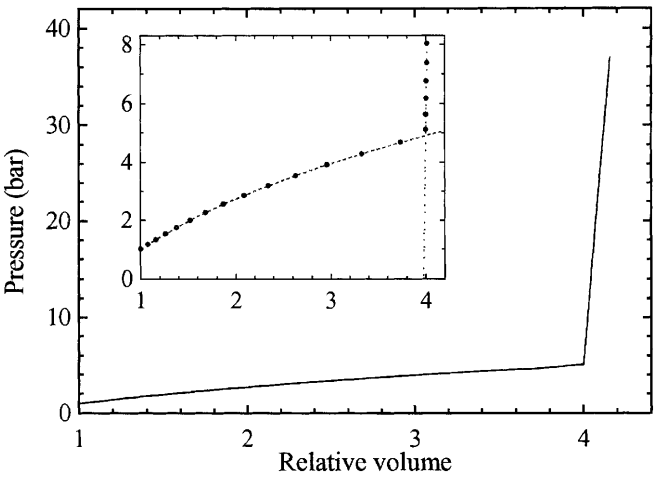

Fig. 2. Pressure vs. relative volume relation for the model cavity. The two parts of the curve correspond to the two regimes in stress–strain behavior of human skin (see text). The enlarged view of the low-pressure range in the *inset* presents analytical relations (4), (8), and (p, V) pairs from Fig. 3

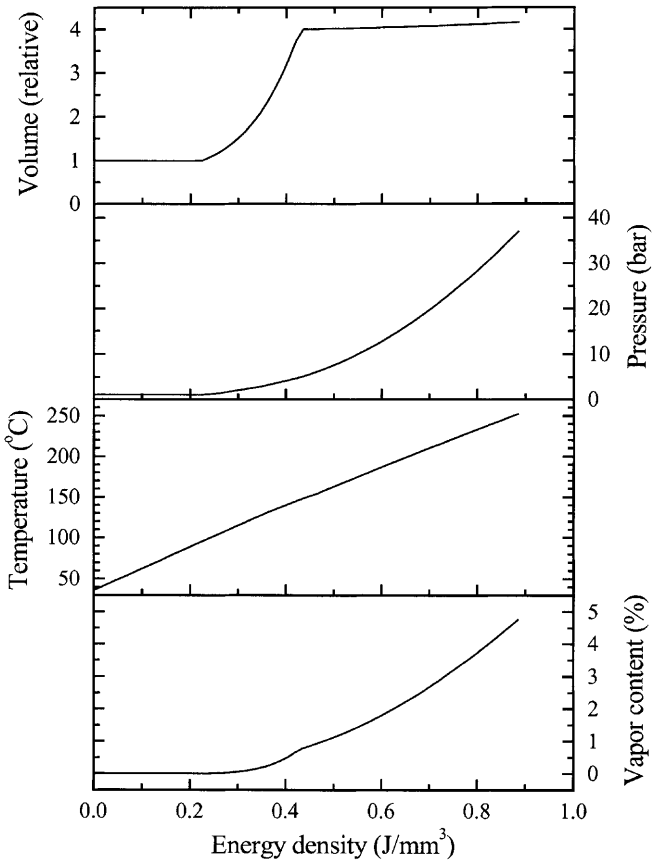

Fig. 3. Cavity volume (relative to the initial volume V_0), pressure, temperature, and vapor content, as a function of delivered energy density. Result of the model using a constant irradiation intensity (10^3 W/cm^2) and zero thermal conductivity

one spatial grid division Δz. For the repetitively pulsed irradiation, the spatial grid spans a depth of 800 μm with a 1-μm spatial resolution, and the time step is increased to 4 μs. The calculation runs up to 5 ms beyond the end of irradiation, which ensures sufficient relaxation of temperature rise and a proper evaluation of thermal damage. In order to minimize the artifacts at the inner boundary of the treated layer, conduction of heat from the last grid point into the depth of the tissue is calculated from the extrapolated thermal gradient.

In all presented cases, the intensity of laser radiation is constant during the laser pulse and the tissue surface is treated as perfectly insulated. This is accomplished by introducing an additional spatial point just outside the tissue surface with the temperature equal to the value at the neighboring superficial point, thus preventing any heat flow through the surface. The calculation is always stopped if pressure p exceeds the ultimate tensile strength of the tissue. At this point the ablation of tissue begins, which can not be treated with the current version of the program.

2 Results

Temperature evolution at different depths within the tissue, as calculated for the case of irradiation with a 300-μs laser pulse, is presented in Fig. 4. The pulse fluence is set to 0.6 J/cm^2, which is close to but still below the ablation threshold at this

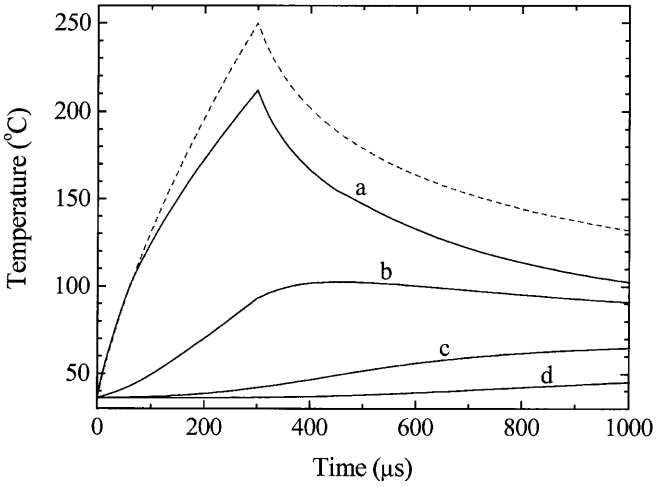

Fig. 4. Temperature development during and after a 300-μs laser pulse at the tissue surface (a), and at depths of 10 μm (b), 20 μm (c), and 30 μm (d). The *dashed line* shows the temperature evolution at the tissue surface according to the ordinary heat-diffusion equation. Pulse fluence: $F = 0.6$ J/cm^2

pulse length, according to our model (see Fig. 7). Although the surface temperature in this case reaches 212 °C, it barely exceeds 100 °C at a relatively shallow depth of 10 μm. At the depth of 20 μm, peak temperature of 67 °C is reached more than 1 ms after the end of the laser pulse. According to (12), protein denaturation can still occur at such temperatures, if they persist for a longer time.

The curves in Fig. 4 are very similar to solutions of the heat-diffusion equation for a semi-infinite homogeneous medium with heat sources distributed exponentially along the isolated surface [26]. A direct comparison shows however, that significantly higher temperatures are predicted, as the latent heat of water evaporation is ignored in this case (dashed line). In contrast to that, the abrupt decrease of slope in our temperature evolution curve (a) clearly demonstrates that at temperatures above 100 °C one part of deposited heat is converted to internal energy of the vapor phase and elastic energy of the strained surrounding medium.

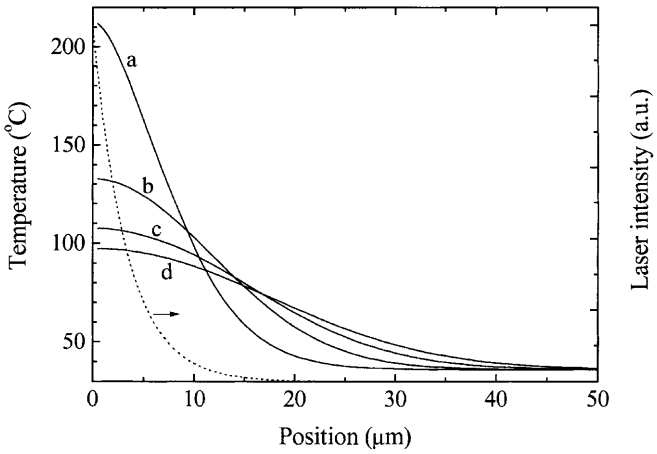

Fig. 5. Temperature profiles within the irradited tissue at the end of a 300-μs laser pulse (a), and at time delays of 600 μs (b), 900 μs (c), and 1200 μs (d) after beginning of the pulse ($F = 0.6$ J/cm^2). The *dotted line* shows the laser intensity distribution for comparison

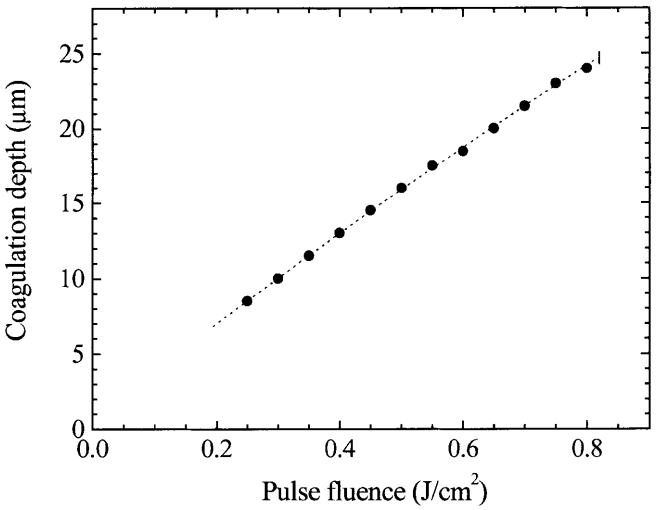

Fig. 6. Fluence dependence of coagulation depth at pulse length of 300 μs. The *dotted line* is a parabolic fit to the results, and the vertical bar marks the ablation threshold fluence

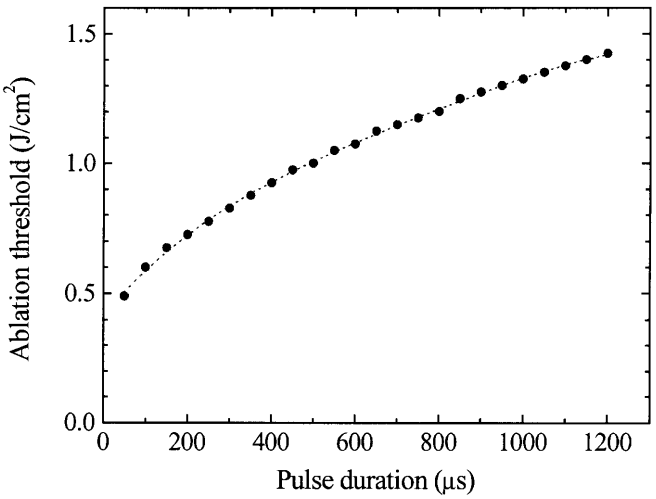

Fig. 7. Ablation threshold fluence as a function of the laser pulse duration. The *dotted line* is a polynomial fit of the third order, not supported by theory

Figure 5 presents the temperature profiles inside the tissue at equidistant times after the end of a 300-μs laser pulse, displaying deeper tissue layers heated to protein denaturation temperatures (60 –70 °C) at relatively late times. A comparison between the temperature profile at the end of the laser pulse (a) and the laser intensity profile (dotted line) illustrates the influence of heat diffusion during such laser pulse.

The extent of thermal coagulation, defined as the depth where Ω equals 0.5, is plotted in Fig. 6 as a function of pulse fluence for the 300-μs pulse. A parabolic fit to the results (dotted line) indicates that below the ablation threshold, the coagulation depth increases virtually linearly with the pulse fluence.

2.1 Influence of the laser pulse duration

Figure 7 presents the influence of pulse duration on the ablation threshold. This relation is obtained by solving the model for increasing pulse fluence (in steps of $0.025\,\mathrm{J/cm^2}$) until the cavity pressure p exceeds the ultimate tensile strength of the tissue, which is repeated at pulse durations from 50 μs to 1.2 ms. From the results, the ablation threshold increases monotonically with pulse lengths from 50 μs on, increasing almost threefold over the examined pulse length range. An ablation threshold value of $0.82 \pm 0.02\,\mathrm{J/cm^2}$ is predicted for the pulse length of 300 μs, typical for medical Er:YAG lasers.

The influence of pulse duration on depth of thermal damage is shown in Fig. 8 for four pulse fluences between 0.6 and $1.2\,\mathrm{J/cm^2}$ (solid symbols). The results show that direct influence of the pulse duration on coagulation depth is minimal, especially at the larger fluences. The four data sets (and the corresponding linear fits) are cut off at the low-pulse-length side, as the ablation regime is reached by shortening the pulse at a fixed fluence value (see Fig. 7).

Since the sub-ablation coagulation depth is maximal at the ablation threshold (see Fig. 6), an envelope to such data sets yields the maximum coagulation depth achievable at a varying pulse duration. This is calculated in more detail by setting

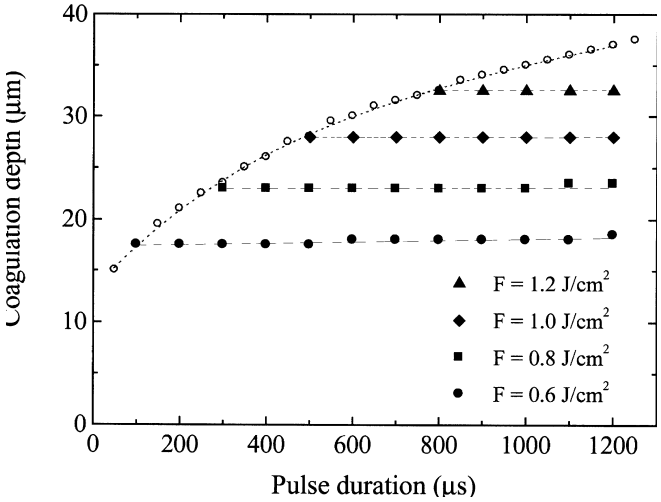

Fig. 8. Coagulation depth as a function of pulse duration at four pulse fluence values (see the legend). Linear fits to the four data sets are shown as *dashed lines*. The *open circles* mark the maximum coagulation depth, calculated by setting the pulse fluence to the ablation threshold value at equidistant pulse durations and the *dotted curve* is a polynomial fit to these data

the pulse fluence to the ablation threshold value at equidistant pulse durations (Fig. 8 - open circles). It increases monotonically from 15 μm at pulse length of 50 μs to 37 μm at 1.2 ms, with a weak saturation at the longest pulses.

2.2 Mechanical properties of tissue

We examine first the dependence of ablation threshold fluence on the ultimate tensile strength of the tissue, which is used explicitly in the ablation onset condition. The results show that the examined dependence is rather weak and practically linear (Fig. 9). With the ultimate tensile strength increased from 2.5 to 4.0 MPa, the ablation threshold rises by just $(17 \pm 1)\%$ at all three pulse durations under test (100, 300, and 900 μs).

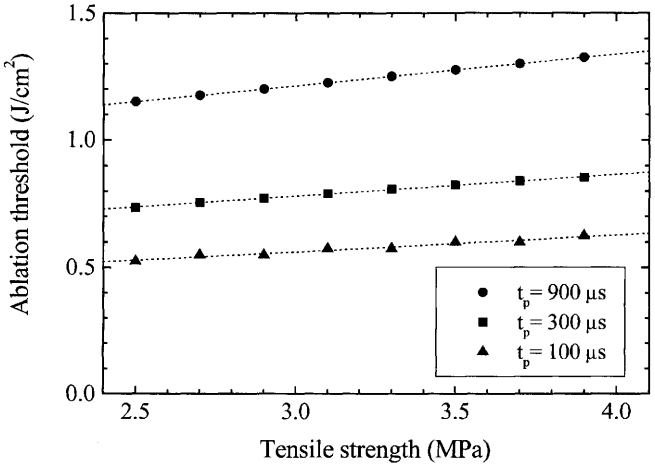

Fig. 9. Influence of the tissue tensile strength on ablation threshold fluence for three pulse durations (see the legend). Linear fits to the three data sets are also shown (*dotted lines*)

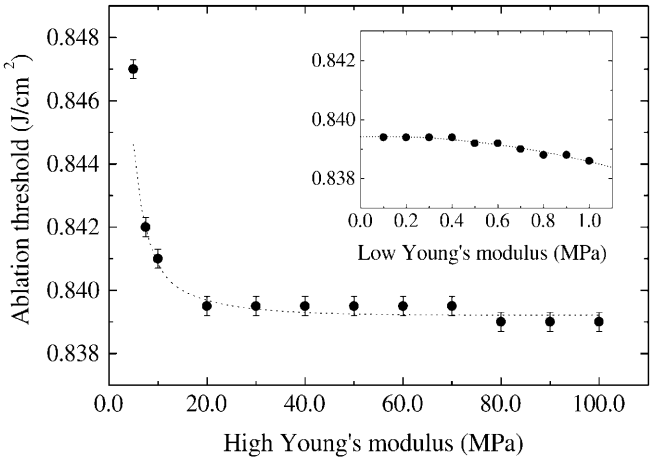

Fig. 10. Dependence of ablation threshold fluence on the higher Young's modulus E_2, and on the lower Young's modulus E_1 (in the *inset*). The *dotted curves* are second-order exponential, and parabolic fit to the data, respectively. Pulse length is 300 μs

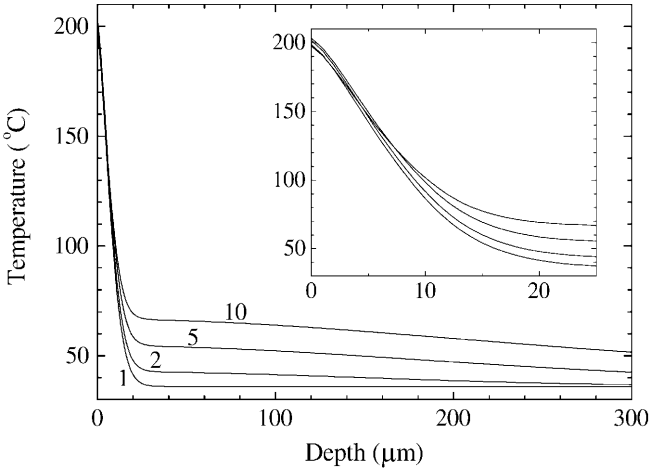

Fig. 11. Temperature profiles at the end of a multiple-pulse sequence with the repetition rate of 10 Hz. Number of pulses in the sequence is given next to each curve. Enlarged view of the superficial layer is given in the *inset*. Single-pulse parameters: $F = 0.6\,\mathrm{J/cm^2}$, $t_\mathrm{p} = 300\,\mu\mathrm{s}$

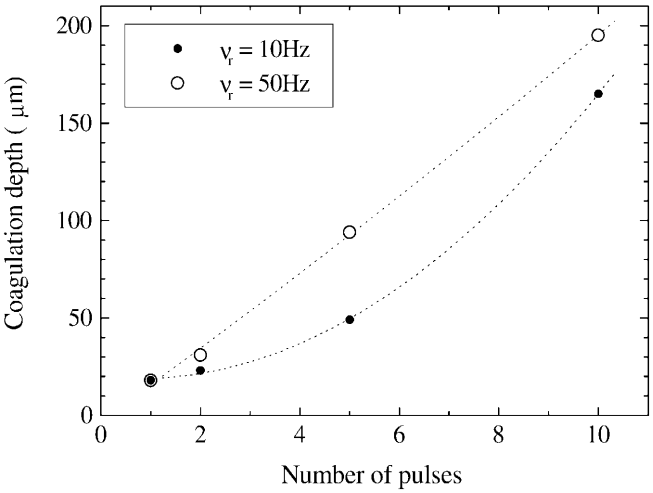

Fig. 12. Depth of coagulated layer as a function of number of pulses for pulse repetition rates of 10 and 50 Hz ($F = 0.6\,\mathrm{J/cm^2}$, $t_\mathrm{p} = 300\,\mu\mathrm{s}$). The two *dotted lines* are parabolic fits to guide the eye

Next, we analyze the influence of the two Young's moduli on the ablation threshold value. Similar to the previous case, this dependence is very weak in a wide range of values (Fig. 10). Especially increasing the higher Young's modulus E_2 (from its value of 48 MPa) has almost no effect, and it must be decreased to less than 20 MPa to result in a small increase of ablation threshold. In contrast, lowering of the lower Young's modulus ($E_1 = 0.5$ MPa) to arbitrarily low values has virtually no effect, and doubling it decreases the ablation threshold by no more than 0.1%.

2.3 Number of pulses

Figure 11 presents temperature profiles within the tissue, as calculated at the end of repetitively pulsed irradiation with 1, 2, 5, and 10 pulses at pulse repetition rate of 10 Hz, single-pulse fluence of $0.6\,\mathrm{J/cm^2}$, and 300 μs pulse duration. The results show that accumulation of heat with repetitive irradiation can be much larger deep within the tissue than at its surface (see the enlarged view in the inset). This can be attributed to differences in temperature gradient, which is very large in the superficial layer of a few laser penetration depths ($1/\mu \approx 3\,\mu\mathrm{m}$), but much smaller deeper inside the tissue (Fig. 11). As a result, the conductive cooling of the interaction layer is very effective, although the tissue surface itself is treated as perfectly insulated. In contrast, deeper tissue layers remain moderately heated for a significantly longer time, owing to weaker heat flow from this region.

Since the protein denaturation rate depends on temperature in a highly nonlinear manner, the amount of thermal damage can not be assessed directly from the presented temperature profiles. For that purpose, denaturation profile $\Omega(z)$ is evaluated during and after the pulse sequence, and the coagulation depth is determined as explained above. The results in Fig. 12 indicate that accumulation of heat in the repetitively pulsed regime enables up to tenfold increase of coagulation depth compared to single-pulse irradiation – even at a moderate repetition rate of 10 Hz.

2.4 Repetition rate

The influence of repetition rate is illustrated in Fig. 13 by comparing the temperature profiles after irradiation with 5-pulse sequences at varying repetition rates from 2 to 100 Hz (single-pulse parameters: $F = 0.6\,\mathrm{J/cm^2}$, $t_\mathrm{p} = 300\,\mu\mathrm{s}$). It is evident that conductive cooling of the superficial layer is much less effective at high repetition rates (see the inset). Nevertheless, relatively deep tissue layers are heated to coagulative temperatures without ablating the tissue surface in all presented cases.

Evaluation of coagulation depth under the same conditions as above shows a nearly linearly increasing coagulation depth with increasing repetition rates up to 20–30 Hz (Fig. 14). At higher repetition rates a strong saturation is observed, effectively limiting the coagulation depth to approximately 100 μm for the 5-pulse sequence.

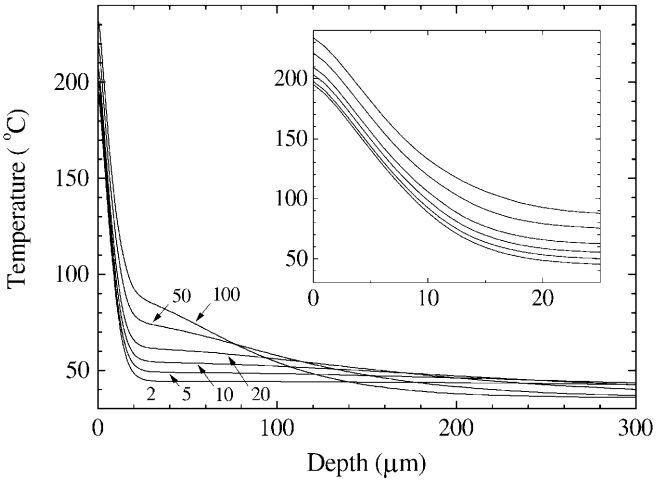

Fig. 13. Temperature profiles after a sequence of 5 laser pulses with repetition rates from 2 to 100 Hz (marked next to the corresponding curves; $F = 0.6\,\mathrm{J/cm^2}$, $t_\mathrm{p} = 300\,\mu\mathrm{s}$). The *inset* shows enlarged view of the superficial layer

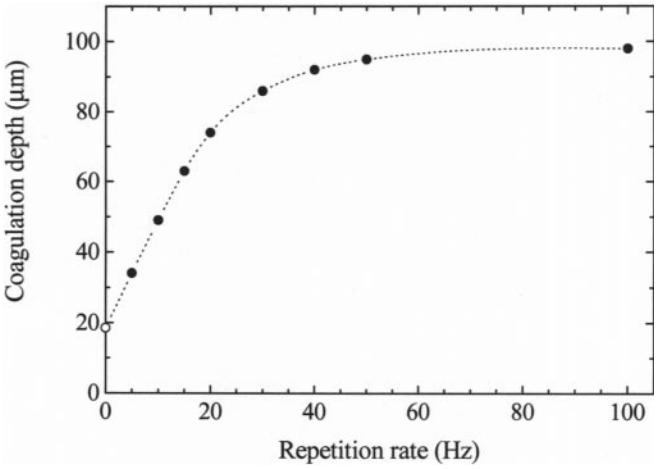

Fig. 14. Coagulation depth obtained with a sequence of 5 pulses with varying pulse repetition rate. Single-pulse ablation threshold, which corresponds to the low-repetition-rate limit, is marked with *open symbol* ($F = 0.6\,\mathrm{J/cm^2}$, $t_\mathrm{p} = 300\,\mu\mathrm{s}$)

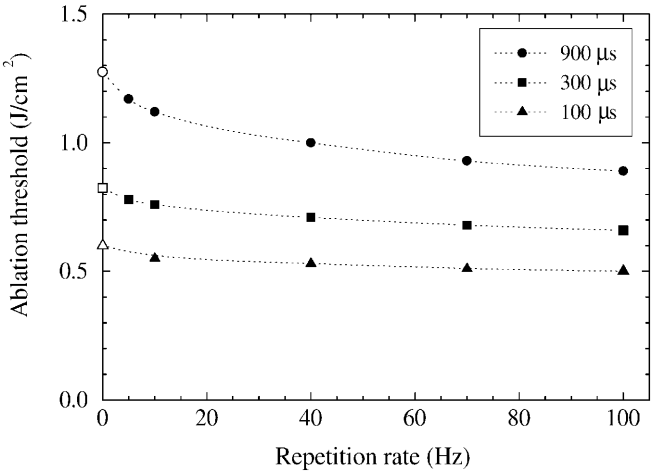

Fig. 15. Ablation threshold fluence for a sequence of 5 laser pulses at varying repetition rate and three pulse durations (see the legend). The *open symbols* mark single-pulse ablation thresholds, corresponding to the low-repetition-rate limit at each pulse duration. The *dotted curves* are a guide to the eye, not supported by theory

Finally, the influence of repetition rate on the ablation threshold is examined for a sequence of 5 pulses with a single-pulse fluence of $0.6\,\mathrm{J/cm^2}$ (Fig. 15). The three data sets, obtained with pulse durations of 100, 300, and 900 μs, are complemented by the single-pulse threshold values (open symbols). These correspond to the low-repetition-rate limit, in which the temperature rise would be completely relaxed between successive laser pulses. The ablation threshold decrease with increasing repetition rate is found to be more pronounced at low repetition rates, especially with longer pulse durations.

3 Discussion

Temperature profiles in Fig. 5 show that diffusion of heat diminishes the superficial temperature rise achieved with a 300-μs laser pulse. As a result, the ablation threshold varies with pulse duration, which holds for the pulse lengths from 50 μs on (Fig. 7). This is in agreement with the commonly used estimate based on analytical treatment of a homogeneous medium, that the influence of heat diffusion is negligible for pulse lengths significantly shorter than the thermal relaxation time. For the discussed case, the latter is estimated to $\tau = (D\mu^2)^{-1} \approx 110\,\mu\mathrm{s}$.

In contrast to that, the coagulation depth is affected only marginally when the pulse duration is varied at a constant fluence value (Fig. 8). We attribute this to the fact that deeper tissue layers (20–30 μm) are coagulated relatively late after the end of the pulse, when the details of initial temperature distribution are already wiped out by the heat diffusion process (see Fig. 5). The strong dependence of maximal sub-ablative coagulation depth on the pulse duration (Fig. 8) thus results primarily from the change in ablation threshold, not from direct influence of heat diffusion. A higher ablation threshold simply enables more energy to be deposited into the tissue without ablating its surface. Since the coagulation depth is known to decrease when the pulse fluence exceeds the ablation threshold value [27, 28, 31], results in Fig. 8 actually represent the maximum coagulation depth achievable overall.

Er:YAG lasers with pulse duration of 200 μs or less thus feature a low ablation threshold and minimal thermal damage, whereas a pulse length of 1 ms or more would be preferred for non-ablative coagulation of deeper tissue layers. Given the limitations of laser physics and technology, coagulation of collagen at depths of 100–200 μm (papillary dermis) seems, however, to be out of reach with single-pulse Er:YAG laser irradiation.

In our model of micro-explosions, the surface temperature at which a given tissue gets ablated is a constant. Its value is obtained by inserting the ultimate tensile strength σ_c for pressure p in (5). For the discussed case of human skin on the face and head, this yields $T_{ab} = 252\,^{\circ}\mathrm{C}$, in good agreement with experimental observations [9, 14].

From the above it also follows, that the ablation temperature does not depend on elasticity of the tissue. Nevertheless, Young's moduli can influence the ablation threshold and efficiency through relations between deposited heat and resulting change of the thermodynamic state of the model cavity (3), (7), (12). The surprisingly weak dependence of the ablation threshold on both E_1 and E_2 (Fig. 10) in our view results from specific elastic properties of skin, which is rather soft at small deformations, but quite stiff at linear extensions above 100% [23]. The p–V diagram of the permitted thermodynamic states of our model cavity (Fig. 2) shows that tissue water initially evaporates almost as in free atmosphere (isobarically), switching to evaporation at a nearly constant volume in the high-deformation regime. As a result, both lowering of the smaller modulus E_1 towards 0, and increasing of E_2, have minimal effect on energy balance of the ablation process. Somewhat stronger influence is observed with increasing E_1 or lowering E_2, but a significant effect is observed only with large changes, when the two values actually become comparable. This implies that the results of the presented model are not affected significantly if the Young's moduli change by a moderate amount. This is very important, since they are known to vary with air humidity, for example [23]. Although this result may be counter intuitive, it has been reported before that modification of skin's elasticity (by gluteraldehyde fixation) has no influence on ablation efficiency [5] – an experimental observation that so far has not been explained or reproduced by a theoretical model. (In contrast, our initial calculations using a single Young's modulus demonstrated a strong influence of its value on the ablation threshold).

Poisson's ratio ν forms a single constant $(1+\nu)/2E$ with the corresponding Young's modulus in both EOS for our model cavity (3), (12). A 20% decrease of ν, for example, is thus equivalent to a simultaneous increase of E_1 and E_2 by 7%. Its influence on the ablation process, which is evidently very small, is therefore not investigated separately. As a matter of fact, the Poisson's ratio for rubber is used in presented calculations, owing to lack of appropriate data.

According to the model, influence of the ultimate tensile strength on ablation threshold is rather weak (Fig. 9). This can be attributed to the nonlinear increase of cavity pressure with delivered energy density in the absence of heat diffusion (Fig. 3). By extrapolating the presented pressure evolution one can estimate that a tissue with two times higher tensile strength would require only 10%–20% more energy deposition to reach the ablation threshold (defined by $p = \sigma_c$). This effect could explain the relatively small variation in experimentally observed ablation thresholds for skin, despite the strong dependence of its tensile strength on air temperature, humidity, and patient age [23].

Figure 3 shows as well that less than 5% of tissue water is predicted to evaporate before the onset of ablation. This justifies our approximation of constant absorption coefficient, thermal conductivity, specific heat and density, which all decrease with reduced amount of liquid tissue water. As this specific run of the model was performed with no heat diffusion, the energy density delivered before the onset of ablation ($0.89 \pm 0.01\,\mathrm{J/mm^3}$) matches the specific heat of ablation h_a by definition. The fact that experimentally determined values are $1.5\,\mathrm{J/mm^3}$ [6, 16] or higher could be attributed to the influence of heat diffusion during the laser pulse, or to the decrease of water absorption coefficient due to temperature rise [29, 30] or tissue desiccation [31].

The feasibility of substantial thermal buildup deep below the surface with repetitively pulsed Er:YAG laser irradiation (Fig. 11) has been demonstrated before by solving the heat-diffusion equation for a semi-infinite homogeneous medium with repetitive heating along its isolated surface [26]. Much more realistic models must be used, however, to predict the amount of thermal damage under such conditions. Our results indicate that the coagulation depth depends on the number of pulses and repetition rate in a peculiar way, reflecting the nonlinear kinetics of both heat diffusion and the protein denaturation process (Fig. 12). When comparing coagulation depths predicted for various application modalities, one should keep in mind, however, that different types of tissue damage might be encountered in the superficial layer even at the same coagulation depth (defined by $\Omega(z) = 0.5$). Such effects could be predicted in part by comparing the damage profiles $\Omega(z)$, but histological investigations are necessary to clarify this issue.

The coagulation depth exhibits a steep initial increase with increasing pulse repetition rate, and a strong saturation above ≈ 40 Hz (Fig. 14). By comparing the temperature profiles at the end of such irradiation sequences (Fig. 13), this can be linked to the fact that at low repetition rates, a large part of deposited energy flows past the region of interest (100 μm in this case), without inducing coagulative temperatures. Higher repetition rates result in shorter irradiation sequences, which confine the deposited heat to a shallower layer. This results in higher temperature rises, and crossing of temperature profiles in Fig. 13. At repetition rate of 50 Hz, for example, the 5-pulse sequence is 100 ms long, and the reach of heat diffusion can be estimated to $(Dt)^{1/2} \approx 100$ μm. At higher repetition rates, most of the deposited heat is thus confined to tissue layer shallower than 100 μm and fully contributes to coagulation of this tissue layer. Note that the maximum coagulation depth achieved with a 5-pulse sequence is roughly 5 times larger than the one achieved with a single pulse (or very low repetition rate), which relates nicely to the linear dependence in Fig. 6.

On the other hand, the conductive cooling of the tissue surface is less effective at higher repetition rates (see the inset in Fig. 13), which results in a decrease of ablation threshold (Fig. 15). As a result, the maximum coagulation depth achievable in sub-ablative mode thus probably peaks at approximately 50 Hz, at least for the treated sequence of 5 pulses.

The presented model may require further improvements to ensure a quantitative match with experimental data on dis-

cussed effects, which are for the most part not available at this time. In our view, the most serious limitations of this model are its inability to treat the removal of tissue (ablation), and the assumption of an isolated tissue surface. The latter holds well for single-pulse irradiation, but with repetitive irradiation, evaporation from tissue surface between consecutive pulses may decrease the temperature [32], and affect the optical and thermal properties in superficial tissue layer. The predicted values for coagulation depths are somewhat questionable, as the lack of experimental data on sub-ablative thermal damage prevented us from determining the optimal Arrhenius coefficients (A, E). Nevertheless, we believe that the model demonstrates beyond a doubt that a superficially ablative regime or a coagulative regime can be accomplished with a repetitive Er:YAG laser by varying the irradiation parameters. Furthermore, the predicted coagulation depths and trends correspond well to first experimental observations [17–19].

Further, the dynamic variation of the tissue absorption coefficient resulting from strong temperature dependence of water absorption [29, 30] is disregarded. Note however, that the value used ($\mu = 300\,\mathrm{mm}^{-1}$) has been determined experimentally under very similar conditions as discussed here [25], and differs significantly from the room-temperature water absorption coefficient ($\approx 1200\,\mathrm{mm}^{-1}$) [29] multiplied by the hydration factor w. Using this absorption coefficient value is probably a key to predicting realistic ablation threshold values. Existence of the partly desiccated superficial layer of skin (stratum corneum) has also been ignored at this point, partly due to lack of information on hydration profile and mechanical properties in this layer.

Finally, describing irradiated tissue by the EOS derived for a single water cavity in an infinite elastic medium is certainly just a convenient starting approximation, used to introduce mechanical effects in a manageable model of thermo-mechanical laser ablation. The fact that tissue water is in reality confined in cavities of different shapes probably requires a different ablation onset condition (relation between p and σ_c), but this is in effect equivalent to modifying the value of σ_c in the existing model. Similarly, the high water content of soft biological tissues results in mutual interaction between the neighboring cavities, which can however for a large part be accounted for by increasing the Young's moduli. In fact, the hypothetical cavities do not even have enough space to double their diameters, which on the other hand corresponds nicely to experimental observation of surface deformation (bulging) before the onset of ablation [9].

4 Conclusions

An original numerical model of thermo-mechanical ablation of soft tissues with mid-IR lasers was developed and implemented. To our knowledge, it is the first one based on a microscopic physical model of micro-explosions, and treats also diffusion of heat (in one dimension), and protein denaturation kinetics in the usual way. From published values for optical, thermal, and mechanical properties of human skin, realistic ablation threshold fluences and surface temperatures are predicted using the model. Heat diffusion was found to reduce the surface temperature and consequently increase the ablation threshold at all pulse lengths above 50 μs. Below the ablation threshold, the coagulation depth increases linearly with the applied laser fluence. The maximum coagulation depth increases with pulse duration, due primarily to increased ablation threshold. The predicted influence of ultimate tensile strength and Young's modulus of the treated tissue on the ablation process is in qualitative agreement with experimental observations.

Feasibility of deep coagulation of skin with the superficially absorbed free-generating Er:YAG laser in repetitively pulsed regime is demonstrated. At a repetition rate of 10 Hz, thermal buildup with successive laser pulses at depths of 20–100 μm is larger than at the tissue surface, and the elevated temperatures persist for a longer time due to lower temperature gradients at these depths. This allows one to extend the coagulation depth, which is limited to 40 μm with single-pulse irradiation, to 200 μm or more. The maximum coagulation depth achievable with a given number of pulses increases steeply with increasing repetition rate, but saturates or even diminishes at repetition rates above 50 Hz. Superficial ablation with minimal amount of thermal damage, or deep non-ablative coagulation can thus be achieved with an Er:YAG laser by choosing the appropriate irradiation parameters. Further improvements of this model may be required to improve the match with experimental data, as more of them become available.

Acknowledgements. This work was supported by the Slovenian Ministry of Science and Technology.

Appendix

Consider a spherical cavity of radius r_0 in an infinite elastic medium. When the pressure in it is increased, displacements of the medium $\boldsymbol{u}(\boldsymbol{r})$ are purely radial from the symmetry reasons:

$$\boldsymbol{u}(\boldsymbol{r}) = u(r)\boldsymbol{e}_r\,. \tag{A.1}$$

Consequently, $\nabla \times \boldsymbol{u} = 0$, and, if other forces acting on the medium are negligible, the equilibrium equation for the elastic medium [20], is reduced to

$$\nabla(\nabla \cdot \boldsymbol{u}) = 0\,, \tag{A.2}$$

indicating that $(\nabla \cdot \boldsymbol{u})$ is constant throughout the medium.

When this is expressed in spherical coordinates, the only non-zero term is the radial one:

$$\frac{1}{r^2}\frac{\partial}{\partial r}(r^2 u) = C\,, \tag{A.3}$$

and a simple integration yields

$$u(r) = C\frac{r}{3} + D\frac{1}{r^2}\,, \tag{A.4}$$

where D is the integration constant. As the displacements must converge towards zero at large radii, the constant C is evidently zero, yielding

$$u(r) = \frac{D}{r^2}\,. \tag{A.5}$$

Constant D is determined from the radial component of the (tensile) stress tensor σ_{rr} at the cavity wall, which equals the cavity pressure p:

$$\sigma_{rr}(r_0) = -p\,. \tag{A.6}$$

By using the standard relation with the strain tensor components ε_{ik} [20],

$$\sigma_{rr} = \frac{E}{(1+\nu)(1-2\nu)}\left[(1-\nu)\varepsilon_{rr} + \nu(\varepsilon_{\phi\phi}+\varepsilon_{\theta\theta})\right], \tag{A.7}$$

which can be calculated from (A.5):

$$\begin{aligned}\varepsilon_{rr} &= \frac{\partial u}{\partial r} = -\frac{2D}{r^3}\,,\\ \varepsilon_{\phi\phi} &= \varepsilon_{\theta\theta} = \frac{u(r)}{r} = \frac{D}{r^3}\,,\end{aligned} \tag{A.8}$$

the radial stress is equal to

$$\sigma_{rr} = \frac{2ED}{(1+\nu)r^3}\,, \tag{A.9}$$

yielding the integration constant value of

$$D = \frac{(1+\nu)\,p\,r_0^3}{2E}\,. \tag{A.10}$$

The displacement function (A.5) is thus

$$u(r) = \frac{(1+\nu)\,p\,r_0^3}{2Er^2}\,, \tag{A.11}$$

and the volume of the cavity can be calculated as:

$$V = \frac{4\pi}{3}\,(r_0 + u(r_0))^3 = V_0\left[1 + \frac{1+\nu}{2E}\,p\right]^3\,. \tag{A.12}$$

The cavity wall starts to tear, and ablation of tissue is assumed to begin, when any stress tensor component exceeds the ultimate tensile strength of the medium. To find out when this happens, the tangential component of the stress tensor must be also calculated [20]:

$$\sigma_{\phi\phi} = \frac{E}{(1+\nu)(1-2\nu)}\left[(1-\nu)\varepsilon_{\phi\phi} + \nu(\varepsilon_{rr}+\varepsilon_{\theta\theta})\right] = -\frac{pr_0^3}{2r^3}\,, \tag{A.13}$$

and the same result is obtained also for $\sigma_{\theta\theta}$. The tangential stress component thus peaks at the cavity wall, just like the radial one (A.9), which is however twice as large, and at this point equals hydrostatic pressure p (A.6). The ablation therefore starts, when the cavity pressure exceeds the medium tensile strength σ_c.

References

1. F. Partovi, J.A. Izatt, R.M. Cothren, C. Kittrell, J.E. Thomas, S. Strikmerda, J.R. Kramer, M.S. Feld: Lasers Surg. Med. **7**, 141 (1987)
2. A.D. Zweig, H.P. Weber: IEEE J. Quantum Electron. **QE-23**, 1787 (1987)
3. A. Sagi, A. Shitzer, A. Katzir, S. Akselrod: Opt. Eng. **31**, 1417 (1992)
4. A. Olmes, H.-G. Franke, E. Bänsch, H. Lubatchowski, M. Raible, G. Dziuk, W. Ertmer: Appl. Phys. B **65**, 659 (1997)
5. J.T. Walsh, T.F. Deutsch: IEEE Trans. Biomed. Eng. **36**, 1195 (1989)
6. J.T. Walsh, T.F. Deutsch: Lasers Surg. Med. **9**, 327 (1989)
7. A.J. Welch: IEEE J. Quantum Electron. **QE-20**, 1471 (1984)
8. J.T. Walsh, T.J. Flotte, T.F. Deutsch: Lasers Surg. Med. **9**, 314 (1989)
9. G.L. LeCarpentier, M. Motamedi, L.P. McMath, S. Rastegar, A.J. Welch: IEEE Trans. Biomed. Eng. **40**, 188 (1993)
10. Y. Domankevitz, N. Nishioka: IEEE J. Quantum Electron. **QE-26**, 2276 (1990)
11. J.T. Walsh, T.F. Deutsch: Lasers Surg. Med. **8**, 264 (1988)
12. B. Majaron, P. Plestenjak, M. Lukač: SPIE Proc. **3192**, 147 (1997)
13. B. Majaron, P. Plestenjak, M. Lukač: SPIE Proc. **3245**, 366 (1998)
14. A.D. Zweig, M. Frenz, V. Romano, H.P. Weber: Appl. Phys. B **47**, 259 (1988)
15. R. Kaufman, R. Hibst: Clin. Exp. Dermatol. **15**, 389 (1990)
16. R. Hibst, R. Kaufmann: Lasers Med. Sci. **6**, 391 (1991)
17. B. Drnovšek-Olup, B. Vedlin: Lasers Surg. Med. **21**, 13 (1997)
18. R. Hibst: private communication
19. To be published elsewhere
20. L.D. Landau, E.M. Lifshitz: *Theory of Elasticity*, 3rd edn. (Pergamon Press, Oxford 1986) pp. 3–16
21. M.C. Potter, C.W. Somerton: *Theory and Problems of Engineering Thermodynamics* (McGraw Hill, New York 1993) p. 233
22. F.C. Henriques, A.R. Moritz: Am. J. Path. **23**, 531, 695 (1947)
23. F.A. Duck: *Physical Properties of Tissue* (Academic Press, London 1990) Chapt. 2
24. W.H. Press, B.P. Flannery, S.A. Tenkolsky: *Numerical Recipes in Pascal* (Cambridge University Press, Cambridge 1990) p. 673
25. G.P. Chebotareva, B.V. Zubov, A.P. Nikitin: SPIE Proc. **2394**, 243 (1995)
26. M. Lukač, B. Majaron, T. Rupnik: Proc. 13th Int. Congr. Laser 97 (Springer, Berlin, Heidelberg 1998) p. 566
27. V. Venugopalan, N.S. Nishioka, B.B. Mikić: J. Biomech. Eng. **116**, 62 (1994)
28. B. Majaron, M. Lukač, B. Drnovšek-Olup, B. Vedlin, A. Rotter: SPIE Proc. **2970**, 350 (1997)
29. G.M. Hale, M.R. Querry, A.N. Rusk, D. Williams: J. Opt. Soc. Am. **62**, 1103 (1972)
30. L.W. Pinkley, P.P. Sethna, D. Williams: J. Opt. Soc. Am. **67**, 494 (1977)
31. B. Majaron, D. Šušterčič, M. Lukač, U. Skalerič, N. Funduk: Appl. Phys. B **66**, 479 (1998)
32. J.H. Torres, M. Motamedi, J.A. Pierce, A.J. Welch: Appl. Opt. **32**, 597 (1993)